



HAL
open science

Alloying electrode coatings towards better magnesium batteries

Clément Pechberty, Arthur Hagopian, Jean-Bernard Ledeuil, Dominique Foix, Joachim Allouche, Jean-Noël Chotard, Olivera Lužanin, Jan Bitenc, Robert Dominko, Rémi Dedryvère, et al.

► **To cite this version:**

Clément Pechberty, Arthur Hagopian, Jean-Bernard Ledeuil, Dominique Foix, Joachim Allouche, et al.. Alloying electrode coatings towards better magnesium batteries. *Journal of Materials Chemistry A*, 2022, 10 (22), pp.12104-12113. <10.1039/D2TA02083A>. <hal-03690170>

HAL Id: hal-03690170

<https://cnrs.hal.science/hal-03690170v1>

Submitted on 18 Oct 2022

HAL is a multi-disciplinary open access archive for the deposit and dissemination of scientific research documents, whether they are published or not. The documents may come from teaching and research institutions in France or abroad, or from public or private research centers.

L'archive ouverte pluridisciplinaire **HAL**, est destinée au dépôt et à la diffusion de documents scientifiques de niveau recherche, publiés ou non, émanant des établissements d'enseignement et de recherche français ou étrangers, des laboratoires publics ou privés.



HAL Authorization

Alloying electrode coatings towards better magnesium batteries

Clément Pechberty,^{1,4} Arthur Hagopian,^{1,4} Jean-Bernard Ledeuil,^{2,4} Dominique Foix,^{2,4} Joachim Allouche,^{2,4} Jean-Noël Chotard,^{3,4} Olivera Lužanin,^{5,6} Jan Bitenc,⁵ Robert Dominko^{5,6,7}, Rémi Dedryvère,^{2,4,7} Jean-Sébastien Filhol,^{1,4} Lorenzo Stievano,^{1,4,7} Romain Berthelot^{1,4,7} *

1 : ICGM, Univ Montpellier, CNRS, ENSCM, Montpellier, France

2 : IPREM, E2S-UPPA, CNRS, Univ. Pau & Pays Adour, Pau, France

3 : LRCS, CNRS UMR7314 Université de Picardie Jules Verne, HUB de l'Energie, 15 rue Baudelocque, 80039 Amiens, France

4 : Réseau sur le Stockage Electrochimique de l'Energie (RS2E), CNRS FR3459, HUB de l'Energie, 15 rue Baudelocque, 80039 Amiens, France

5: Department of Materials Chemistry, National Institute of Chemistry, Hajdrihova 19, 1000 Ljubljana, Slovenia

6: Faculty of Chemistry and Chemical Technology, University of Ljubljana, Večna Pot 113, 1000 Ljubljana, Slovenia

7 : Alistore-ERI, CNRS FR 3104, Hub de l'Energie, Rue Baudelocque 80039 Amiens, France

Corresponding author

Dr. Romain Berthelot

romain.berthelot@umontpellier.fr

Institut Charles Gerhardt de Montpellier (CNRS, UM, ENSCM)

Pôle Chimie Balard – 1919, route de Mende, 34293 Montpellier cedex 5 – France

Highlights

- Alloy coating on magnesium surface enables using chloride-free electrolyte
- Mg_2Ga_5 alloy is the main component of the surface layer after reaction with liquid gallium
- Improved metal plating/stripping is obtained with Ga-protected Mg electrodes using $Mg(TFSI)_2/DME$ electrolyte
- The underneath Mg plating is rationalized by DFT calculation
- The coating enables enhanced cycling of magnesium full cells with both sulphur- and organic-based composites as positive electrode

Keywords

Magnesium batteries, Surface protection, Alloy-type materials, Plating/stripping, Mg/S battery, Organic electrodes

Abstract

Mastering the metal-electrolyte interface is mandatory for the development of reliable rechargeable magnesium batteries. Nevertheless, most of the current electrolytes contain chlorides species to bypass the surface passivation of magnesium, making them corrosive to other cell components and potentially irrelevant for industrial application. Here, we demonstrate a novel approach to bypass the use of such electrolytes *via* the mediation of an alloy-type interface prepared by coating the surface of a magnesium electrode with liquid gallium. The chemical alloying induces the formation of a surface layer, mainly composed of the intermetallic Mg_2Ga_5 , enabling significantly improved electrochemical performance with a simple chloride-free $Mg(TFSI)_2/DME$ electrolyte. Sensibly less-polarized and more stable plating/stripping is observed with symmetric cells, and longer cycle life is achieved in full cells

with positive electrodes based on sulphur- and organic composites. This alloy-based surface protection opens the door to electrolytes firstly considered as non-compatible with magnesium metal, and consequently paves the way to the application of metal electrodes in practical magnesium batteries.

Introduction

Lithium-ion batteries have revolutionised the field of energy storage. At the root of the constant electrification of our societies by powering mobile electronics, now they equip new generations of hybrid and electric vehicles and are also considered for stationary storage of renewable energies. Consequently, the global battery production is significantly increasing and sustainability issues might arise even with implementing efficient battery recycling. In this regard, alternative electrochemical storage systems that offer high energy density together with reduced cost and low environmental footprint must be developed. Magnesium batteries, belonging to so-called post-lithium-ion systems, have attracted significant attention since the first rechargeable cell prototype was reported by Aurbach and co-workers.¹ Indeed, using magnesium as the negative electrode theoretically enables high energy density batteries, thanks to the low density of magnesium, the low redox potential of the Mg^{2+}/Mg couple and the doubled charge carried by Mg^{2+} cations.²⁻⁴ In addition, magnesium is abundant and cheap, safer than lithium, and already widely processed on industrial scale. In spite of these promising features, magnesium batteries are still far from a realistic application.

One of the reasons for such delayed commercialization is rooted in the passivation film created on the surface of magnesium electrode in contact with common aprotic battery electrolyte solvents which, unlike lithium metal, inhibits the reversible plating/stripping process of magnesium.^{5,6} In the last 20 years, many electrolyte formulations have been proposed to bypass this major hurdle, from the early use of Grignard reagents to solutions employing borate-based

magnesium salts.^{4,7,8} Unfortunately, despite significant improvements, no miracle formulation coupling good electrochemical performance with low-cost, easily scalable production and eco-friendly properties has been found until now. Only the use of chlorides species enables breaking the passivation layer, however making the electrolytes corrosive and consequently not suitable for real applications.

Mastering the interface between magnesium and electrolyte is then crucial. In 2018, Ban and co-workers designed a polymeric coating combining thermal-cyclized polyacrylonitrile and magnesium trifluoromethanesulfonate, and succeeded in further employing carbonate-based electrolytes.⁹ An organic coating made of reduced perylene diimide-ethylene diamine (rPDI) also enabled fast and reversible magnesium plating/stripping with the chloride-free electrolyte Mg(TFSI)₂/DME.¹⁰ Moving to the inorganic coatings, the teams of Nazar and Archer almost simultaneously proposed the protection of lithium and sodium electrodes by an alloy-type coating, created through the chemical reduction of a metallic salt in solution, followed by an alloying reaction with the alkali metal surface.¹¹⁻¹⁴ Eventually, the passivating film formed in this way is in reality a composite layer, as insulating by-products are also present and offer a potential gradient to prevent plating onto the coating layer. The as-protected electrodes exhibit enhanced electrochemical performance, mainly induced by the minimised dendritic growth during plating.¹⁵ Although magnesium dendrites are not unexpected,¹⁶⁻¹⁸ similar protocols were thus applied to magnesium electrodes with the objective of using more conventional electrolytes. For example, in contact with a SnCl₂ or BiCl₃ solution, a composite layer containing the Mg₂Sn or Mg₃Bi₂ alloy covers the magnesium electrode surface and enables fast ion transport.^{19,20} The creation of such a protective layer could be achieved by modifying the electrolyte formulation with the addition of GeCl₄.²¹ Despite significantly improving the electrochemical performance, using chloride species remains questionable with respect to possible corrosion side reactions with other components of the cell.

An alternative coating strategy, recently proposed for the alkali metals, is the direct reaction with a liquid metal. Protective layers of alkali amalgams were thus obtained on the surface of lithium, sodium and potassium, respectively, by reaction with mercury drops. The as-protected electrodes exhibit an improved electrochemical behaviour such as less severe dendritic growth and improved stability towards moisture.^{22–24} However, the well-known toxicity of mercury precludes any chance of realistic applications. Furthermore, the very high density of the obtained amalgams would dramatically lower the theoretical specific energy density of possible full cells.

Searching for other lighter and environmentally-friendly liquid metals, we demonstrate in this work the feasibility of protecting the surface of magnesium electrode with a gallium-based coating. Gallium has a relatively low abundance on Earth's crust, but is very widely spread as trace element and is generally obtained from processing to produce aluminium or zinc, and good recyclability enables its wide use in electronics industry.^{25–27} Moreover gallium and has been shown to be compatible with magnesium electrochemistry. Indeed, magnesium electrochemically alloys with gallium to form Mg_2Ga_5 . Like other alloy-type electrodes,²⁸ the reaction occurs at low potential (~ 200 mV) and offers high specific capacity (~ 300 mAh/g). In addition, a self-healing behaviour is observed due to the near-room-temperatures solid–liquid phase transformation between solid Mg_2Ga_5 and liquid gallium.²⁹

As shown hereafter, the chemical reaction between liquid gallium and magnesium forms an alloy layer mainly composed of Mg_2Ga_5 at the surface of the electrode. With the chloride-free electrolyte $Mg(TFSI)_2/DME$, while the strong surface passivation of uncoated magnesium electrode significantly alters the electrochemical activity, the as-protected magnesium electrodes exhibit enhanced performance. Consequently, extended cycling is achievable with full cells with various positive electrode composites. The liquid metal coating appears then as a promising strategy and may open the door to realistic application of magnesium batteries.

Surface alloying of magnesium anode

The low melting point of gallium (29.8 °C) enables its easy melting before spreading drops on the surface of a magnesium electrode in an argon-filled glovebox. The metallic shiny aspect of magnesium rapidly evolves and turns grey after few hours (Figure 1a). Multiple surface layers could be evidenced on cross-section scanning electronic microscopy (SEM) images. Starting from the surface, we can distinguish a first thick layer of around 10 – 30 μm, then an oxygen-rich very thin layer (200 – 300 nm) and lastly an irregular micrometric sublayer (1 – 2 μm) observed at the interface with the magnesium bulk electrode (Figure 1b, e and f). Elemental cross-section mapping by scanning Auger microscopy (SAM) shows distribution of gallium and magnesium through the interfaces. Semi-quantitative analysis based on the relative intensities of the Auger spectra of selected areas and their derivatives curves, taking into account the relative sensitivity factors of Mg KLL and Ga LMM lines, unambiguously reveals a richer gallium content in the thick top layer than in the sublayer (Figures 1e-g). The oxygen-rich thin interlayer most probably originates from the native oxide/carbonate surface layer that cannot be fully removed even when operating in glovebox, as shown later by XPS, and possibly from contamination during sample preparation.

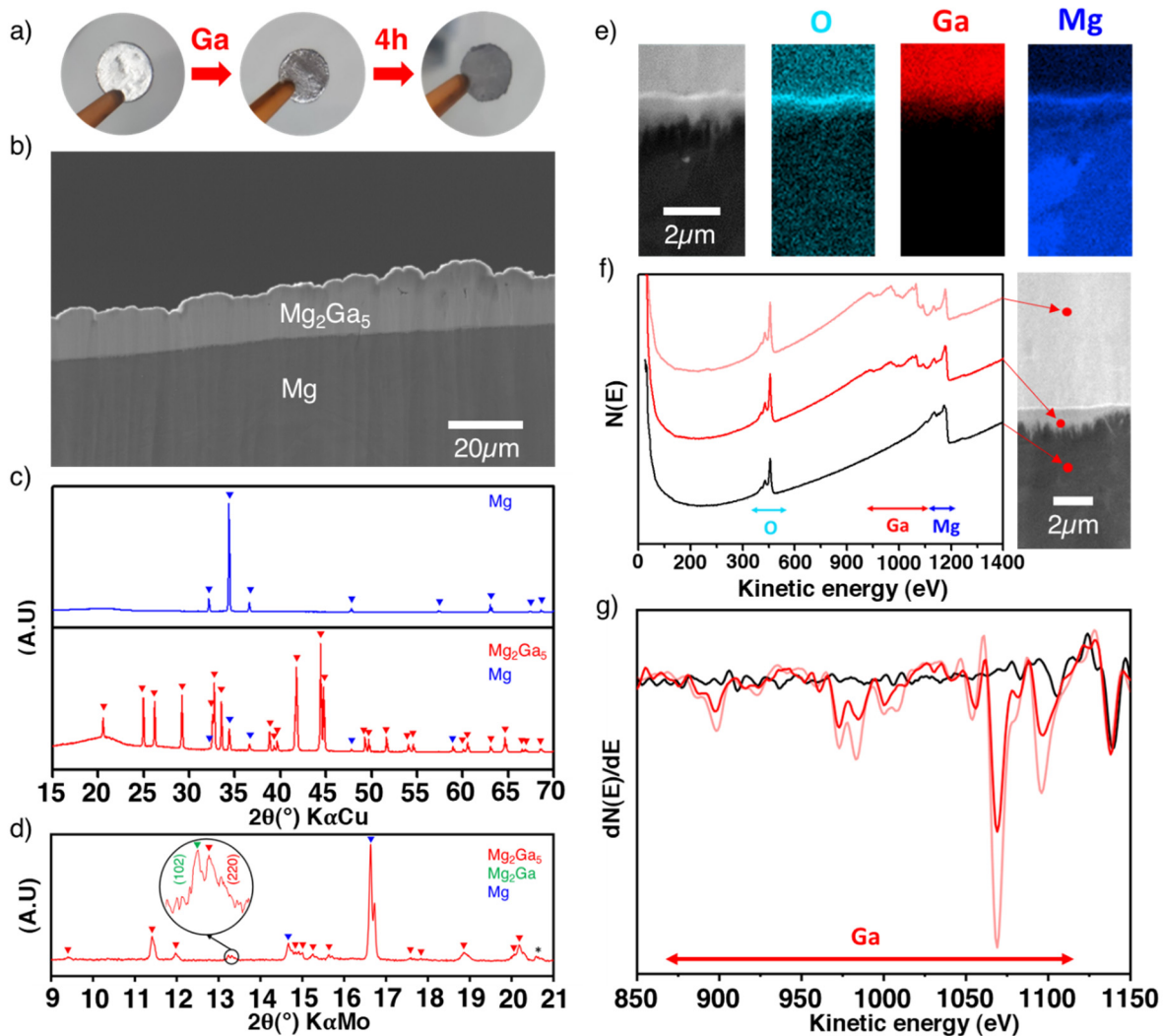


Figure 1. Multi-technique characterizations of the Mg-Ga alloy coating. Pictures of magnesium discs showing the colour changes after reaction with the liquid gallium (a), SEM cross-section image of Ga-treated magnesium disc (b), XRD patterns of bare and treated discs in reflection and transmission modes (c and d, respectively) with peak identification and a special enlarged view to detect the (102) peak of Mg_2Ga ; SAM mapping of O, Ga and Mg elements at the interface (e), Auger electron spectra of selected areas in direct mode “ $N(E)$ ” and derivative mode “ $dN(E)/dE$ ” displaying the chemical composition changes (f and g)

X-ray diffraction was used to get more insights into the coating. The formation of highly crystalline Mg_2Ga_5 is evidenced in reflection geometry (Figure 1c), with refined cell parameters in line with the literature ($I4/mmm$, $a = 8.646(1) \text{ \AA}$ and $c = 7.126(1) \text{ \AA}$, Figure S1) while a

second acquisition performed in transmission geometry with a high brilliant rotating anode source using Mo-K α radiation enables the detection of an additional contribution (zoom in [Figure 1d](#)) that could be reasonably attributed to the (102) peak of Mg₂Ga, a Ga-richer composition of the Mg-Ga phase diagram ([Figure S2](#)). Overall, in agreement with the gallium concentration gradient evidenced by Auger spectroscopy, the thickest top layer and the sublayer below can be reasonably assigned to Mg₂Ga₅ and Mg₂Ga, respectively, as the latter is only detected in transmission geometry.

On the practical side, while controlling the weight of the gallium drops is not straightforward, the thickness of the deposit can be manually tuned during the coating process by adjusting the amount of gallium drops and/or by subsequently wiping out some gallium. Following this procedure, the electrode mass increase after gallium addition experimentally ranges from 18 to 56 %. By simply considering the formation of only Mg₂Ga₅, this mass uptake corresponds to an average layer thickness around 15 to 60 μm ([Figure S3](#)), in good agreement with our SEM observation. Importantly, owing to the molecular weight and density of magnesium, the coating formation does not consume an important volume of magnesium electrode.

Benefits on the electrochemical behaviour

Unlike alkali metals, magnesium is not ductile and cannot be pressed and flattened on the surface of a current collector. Consequently, it appears necessary to cover both sides of each magnesium disc electrode before performing any electrochemical tests. For a better understanding of the magnesium plating and stripping, galvanostatic polarization measurements were first carried out in symmetric cells. With uncoated magnesium electrodes, after an initial peak, the overpotential is rapidly stabilized around 0.6 V during the first polarization sweep. However, in the subsequent ones the galvanostatic profile is strongly modified and the overpotential remains around 2 V, indicating a strong impedance of the

plating/stripping process due to the surface passivation and with consequently cycling failure generally after 100 hours (Figure 2a).

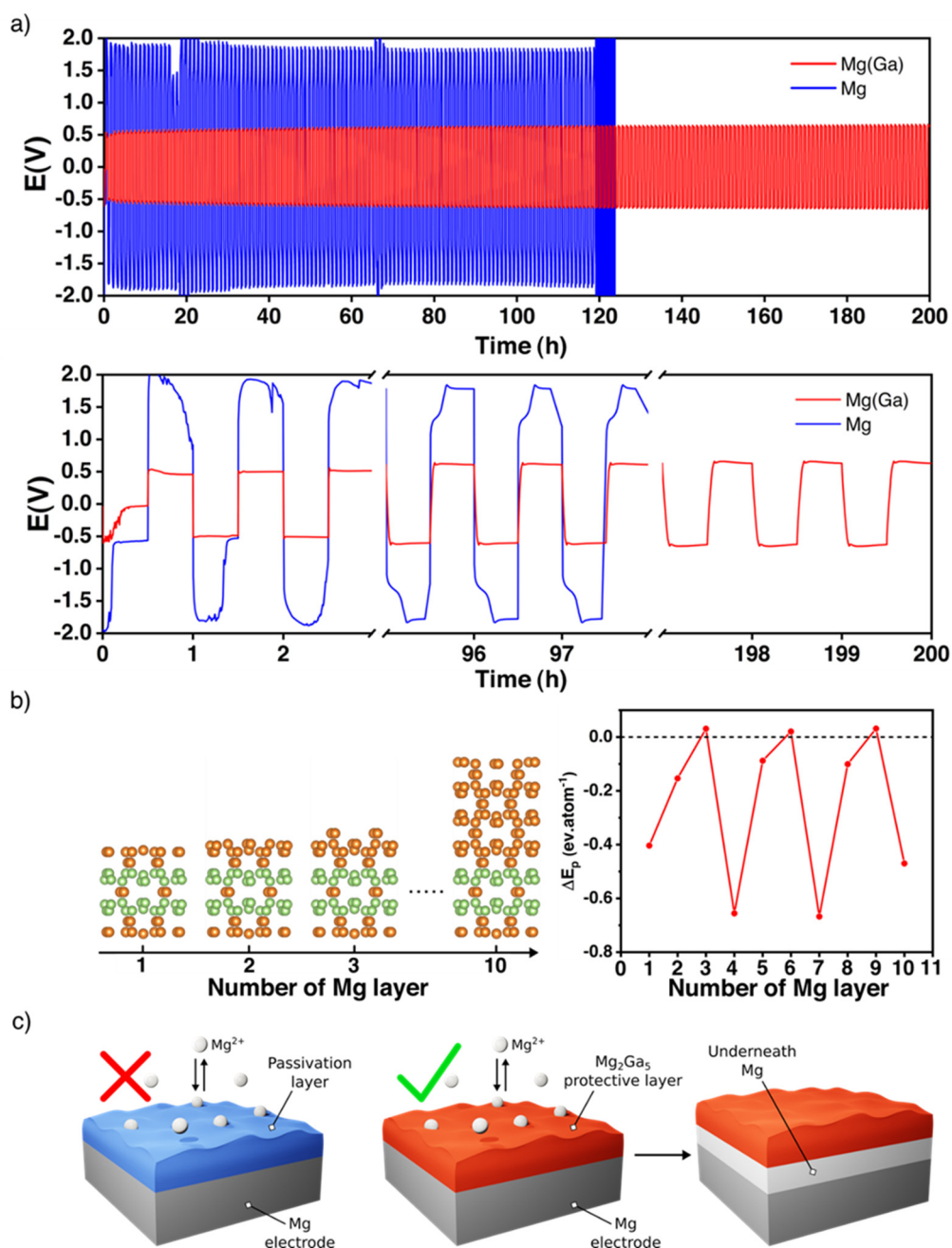


Figure 2. Enhanced magnesium plating/stripping. Development of overpotentials during subsequent magnesium plating/stripping processes in symmetrical cells with bare and Ga-protected magnesium electrodes (blue and red lines, respectively) in 0.8 M $Mg(TFSI)_2/DME$ electrolyte and at 40 °C, with sweeps of 30 min at a current density of $100 \mu A/cm^2$ (a); Structures of magnesium epitaxial surface on Mg_2Ga_5 with increasing number of layers and corresponding DFT-calculated plating energy (b) and schematic representation of an underneath plating (c)

The picture is significantly different with gallium-protected magnesium. The overall overpotential remains around 0.5 V, and the profile is stable for several hundreds of cycles. In detail, each sweep exhibits a weak nucleation peak followed by a flat plateau throughout the whole electrochemical process. It is worth pointing out that a highly concentrated electrolyte was employed, and that the metastability of Mg(TFSI)₂ is known to strongly participate to the surface passivation of magnesium.^{30,31} Despite that, the value of the overall potential is in line with previous works where less concentrated electrolytes are used (Table S1).

In the literature, the charge transfer and the plating mechanism processes occurring at the surface of these coated electrodes are not yet fully understood.¹⁵ The presence of insulating by-products (mainly chlorides) in the composite layers was proposed to create a potential gradient, further enabling the ionic diffusion across the coating and leading to plating occurring below the coating layer, further denoted as underneath plating.¹¹ Moreover, the existence of chloride species dissolved in the electrolyte has been suggested to prevent further passivation through the formation of surface adsorbed species.³² With our coating approach, the protective surface layer is mainly composed of the alloys Mg₂Ga₅ and Mg₂Ga. Density of states obtained from density functional theory (DFT) calculation confirm the metallic state of the alloys (Figure S4). The oxygen-rich layer might be insulating but its influence could be discarded given its narrow thickness. As previously done for lithium systems,^{33,34} DFT calculation was applied to rationalize the magnesium plating onto our Ga-coated electrode. Here, the stability of the different Mg₂Ga₅ surfaces was first analyzed as a function of the surface orientation and the applied potential. As a result, the (001) surface is found to be the most stable one in the potential range of interest (Figure S5). Then, the plating energy ΔE_p , *i.e.*, the energy difference between a magnesium layer epitaxially plated on Mg₂Ga₅ and the same amount of Mg atoms in their bulk environment, was computed for an increasing number of adsorbed layers in order to

qualitatively link the plating mechanism with the current rate, as the greater the current density, the larger the number of Mg atoms accumulated on the coating surface (Figure 2b, see details in the Methods section and Supporting Information).

Most of the magnesium adsorbed layers configurations lead to a strongly negative ΔE_p , suggesting an underneath plating mechanism favorable independently of the current rate. Note that only the 3-, 6- and 9- layers configurations possess a slightly positive plating energy, well below room temperature $k_B T$. Therefore, for such configurations, the surface plating is either unstable or metastable at low temperature. At room temperature, because of the extremely weak surface stabilization, even the metastable Mg layers should dissolve into the Mg_2Ga_5 coating because of both entropic (defects creation) and enthalpic (increase of the number of the strong Mg-Ga bonds relatively to the weaker Ga-Ga ones) effects. To summarise, from a thermodynamic point of view, a magnesium layer epitaxially plated above the Mg_2Ga_5 coating is expected to migrate underneath it to form a magnesium bulk layer at the electrode surface. The physical reason for such behaviour can be revealed through the competition between the adsorption energy and the epitaxial stress. The chemical bond between the adsorbed Mg-layer and the Mg_2Ga_5 substrate appears weak, with an adsorption energy of only -0.12 eV/atom, and cannot compensate the epitaxial stress of the Mg-layer which is constrained to the Mg_2Ga_5 crystallographic environment ($+0.22$ eV/atom).

To confirm the underneath plating suggested by the electrochemical results and the DFT calculation, the evolution of the Ga-coated electrode during repeated plating and stripping cycles was followed *in situ* by XRD in transmission mode. Indeed, the Mg_2Ga_5 layer is highly crystalline and any structural evolution should be detectable in this way. The use of rotating Mo anode enables collection of high-quality diffraction patterns with relatively short

acquisition time (3 minutes), allowing us to follow precisely any changes occurring through the whole electrode (bulk magnesium, alloy coating and the interface with the liquid electrolyte).

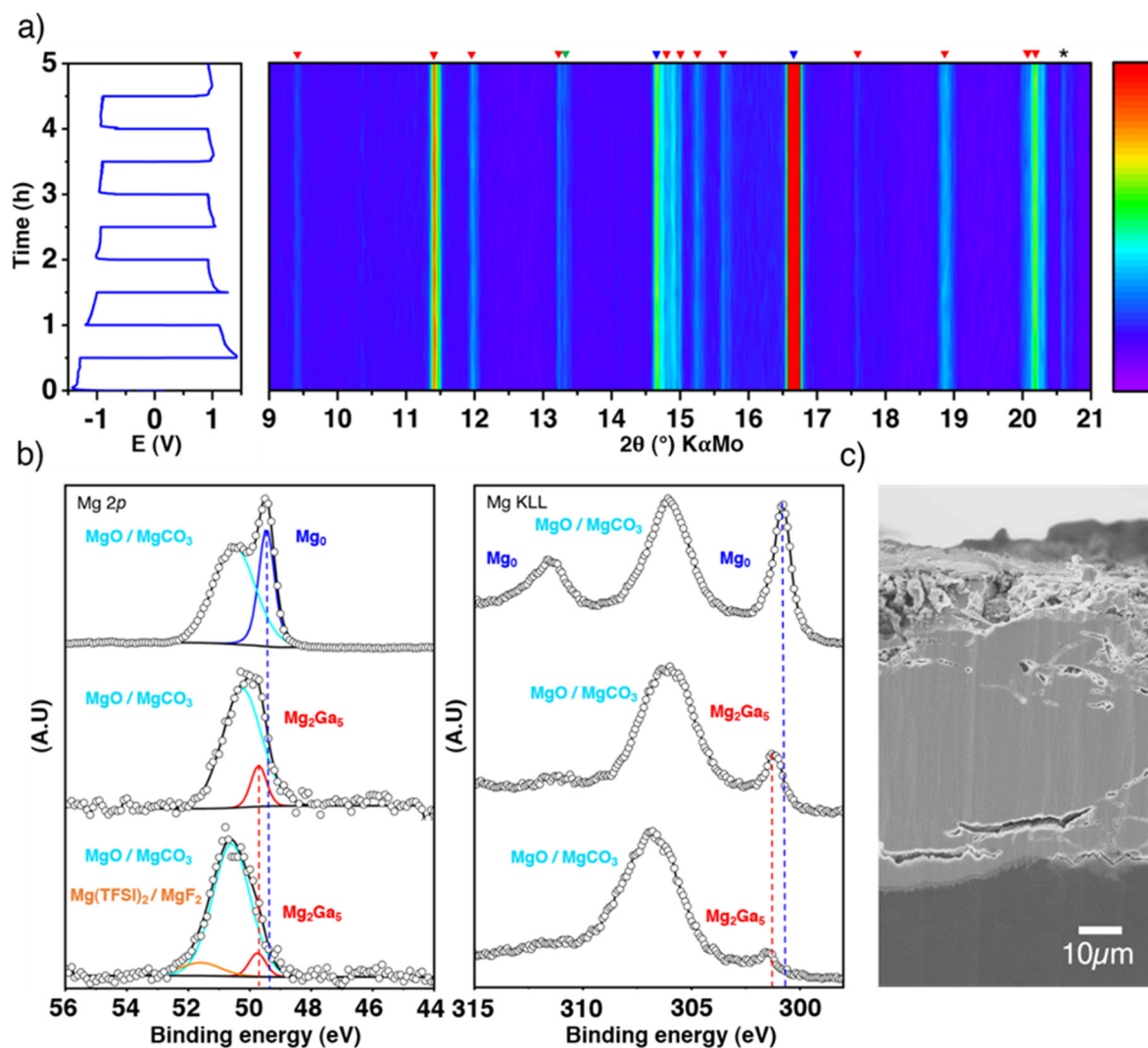


Figure 3. Inside the coating evolution. Top-view representation of XRD patterns collected in situ in transmission mode during galvanostatic polarization measurements of a symmetric cell, with blue, red and green markers for Mg, Mg₂Ga₅ and Mg₂Ga, respectively (a); XPS spectra (Mg 2p and Auger Mg KLL) of pristine Mg, Ga-coated Mg before and after 50 hours of plating/stripping, normalized by the most intense contribution (b); SEM cross-section image of coated electrode after plating/stripping (c). Note that XRD acquisitions were performed at room temperature as the in situ cell does not allow working at 40 °C, even if the coating efficiency is not optimized at such temperature (Figure S6).

At a first glance, the pristine highly crystalline Mg_2Ga_5 and the secondary diffraction peaks assigned to Mg_2Ga remain unmodified all along the electrochemical process (Figure 3a). Only a tiny peak broadening is observed, which can be linked to a decrease of crystallinity and/or increase of lattice strain of the Mg_2Ga_5 crystallites (Figure S7). Focusing now on the composition of the electrode surface, *ex situ* XPS analysis was performed on coated magnesium before and after polarization tests (Figure 3b). The presence of Mg_2Ga_5 alloy for Ga-coated magnesium is evidenced by a significant shift of the thin Auger Mg KLL metallic signature (301.8 eV compared to 301.2 eV for bare magnesium). Due to the greater amount of oxide and carbonate at the surface of the Ga-coated Mg, the relative contribution of the alloy *vs.* MgO/MgCO_3 decreases, which can be observed in the Mg 2p spectrum as well. After 50 hours of successive plating and stripping, Mg_2Ga_5 remains present as no shift of the peak is observed. Magnesium metal is consequently not plated above the coating, in agreement with *operando* XRD and DFT calculations. Additionally, the presence of $\text{Mg}(\text{TFSI})_2$ salt and its degradation product MgF_2 can be also observed in the Mg 2p spectrum (additional XPS spectra of F 1s and Ga 3d are also provided in Figure S8). Finally, cross-section electron microscopy collected *ex situ* also after 50 hours of plating and stripping reveals a global resistance of the coating in spite of some changes in the morphology, with the apparition of cracks in some parts of the protective layer (Figure 3c).

Towards better magnesium batteries

The gallium alloy coating was shown to enhance the electrochemical features and to remain chemically constant during polarization measurements. The coated magnesium electrodes were then evaluated in full cell configuration using the same $\text{Mg}(\text{TFSI})_2$ -based electrolyte. We first considered the Chevrel phase Mo_6S_8 prepared by conventional procedure (Figure S9) as the standard electrode material for magnesium-based batteries for which the electrochemical

activity with magnesium is well established.^{1,35,36} However, Mo₆S₈ is characterised by a relatively low reversible capacity and by a low working voltage and therefore cannot be considered for realistic applications. Galvanostatic profiles obtained with bare and protected magnesium electrodes appear quite similar in the first cycles with two typical plateaus assigned to distinct insertion sites of magnesium ions in the sulphide framework (Figure 4a-b). Electrolyte decomposition parasite reactions could explain the exceeding initial discharge capacity and certainly induce the increasing polarization which causes battery failure after a few cycles. Remarkably, the potential values of the plateaus are very close for both cells, either in charge or in discharge. This is another observation that supports the role of the alloy layer as a composition-invariant coating. Indeed, the potential is significantly lower with negative electrode of bulk Mg₂Ga₅ prepared by mechanical alloying with a difference of 200 mV (*i.e.*, approaching the potential of alloying/dealloying process of gallium²⁹) (Figures S10-11).

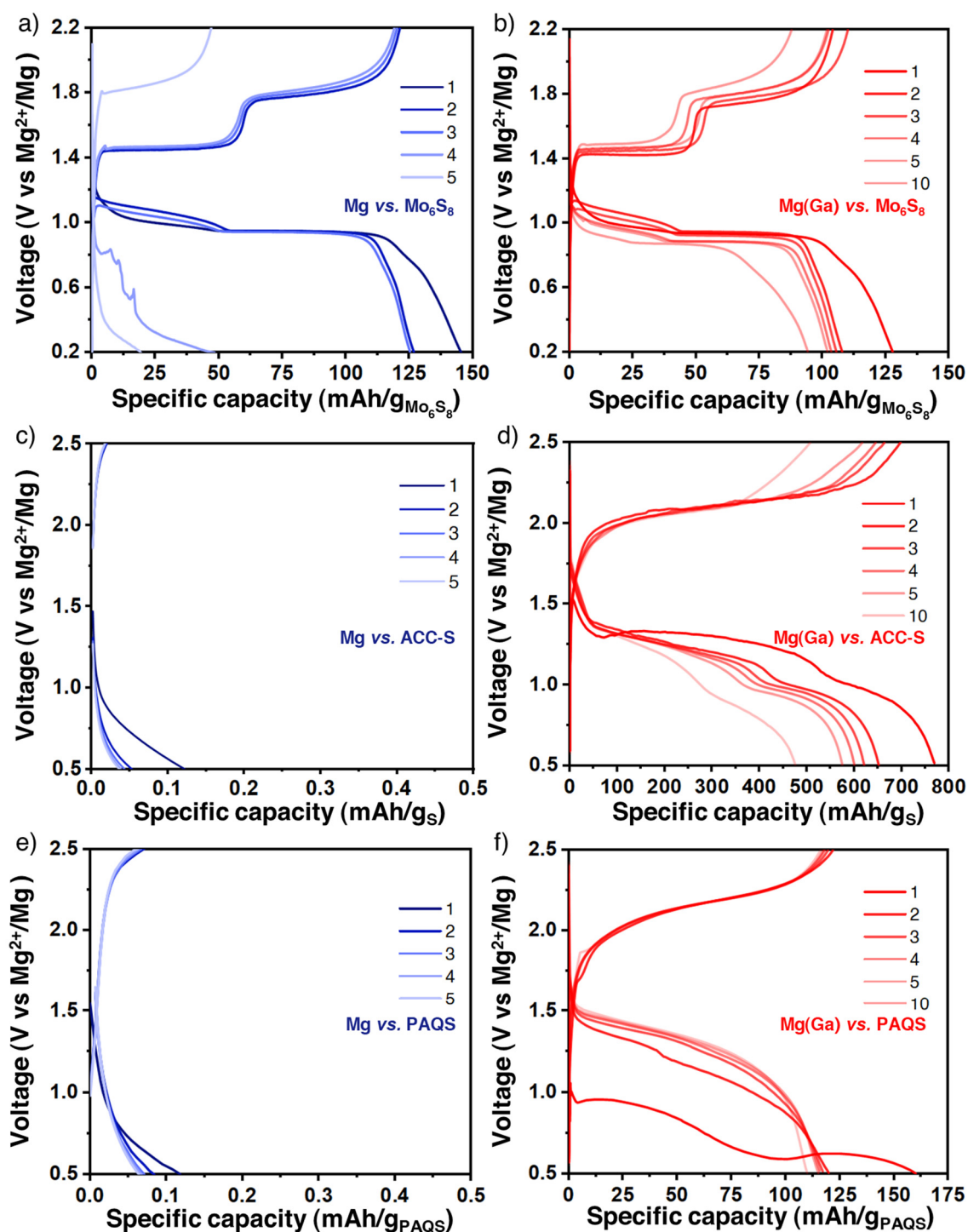


Figure 4. Enhanced cycling in full magnesium batteries. Galvanostatic profile of magnesium batteries with bare and coated magnesium electrodes (blue lines, left, and red lines, right, respectively) assembled successively with different positive electrode: Mo_6S_8 (a and b, at C/10 or 6 mA/g), carbon-sulphur composite ACC/S (c and d, at C/10 or 167 mA/g) and carbon-organic composite PAQS-CNT (e and f, at C/2 or 122 mA/g). Batteries tests performed at 40 °C.

On the road towards realistic magnesium batteries, sulphur- and organic-based composites are then considered. Indeed, given the sluggish diffusion of Mg^{2+} ions in classical insertion hosts such as high-voltage layered oxides or polyanionic compounds, working with sulphur, a conversion-type electrode, is a promising pathway and Mg/S cells could potentially exhibit high energy density while meeting sustainability and durability criteria.^{37–39} Nevertheless, the well-known intrinsic drawbacks of sulphur-based electrodes, from the insulating character of sulphur to the well-known polysulphides shuttle effect, could lower these promising values and therefore still need to be overcome. Besides sulphur, organic compounds are now regularly highlighted as possible cathode materials in divalent batteries, mainly quinone derivatives involving a carbonyl group as redox centre. Despite the solubility issue, which can be mitigated with polymer synthesis, promising electrochemical cycling could be obtained with appropriate electrolytes.^{40–47} We used sulphur-impregnated activated carbon clothes (ACC-S, [Figure S12](#)) which are commonly used as model electrodes in magnesium batteries despite their limited sulphur loading (10 wt.% of sulphur, corresponding to a surface density around 1 mg/cm^2).^{48–}
⁵⁰ In parallel, the popular redox polymer poly (anthraquinonyl sulphide) (PAQS, [Figure S13](#)) was chosen due to its reversible electrochemical mechanism with divalent ions with $\text{Mg}(\text{B}(\text{hfp})_4)_2$ and $\text{Mg}(\text{TFSI})_2\text{-}2\text{MgCl}_2$ electrolytes and combined with carbon nanotubes (CNT) for improved capacity utilization.

For both electrode composites, the comparison between bare and protected magnesium electrode strikingly highlights the benefits of the alloy coating. The strong passivation of magnesium metal induces an immediate cell failure ([Figure 4c-d](#) for ACC-S and [e-f](#) for PAQSD-CNT). On the contrary, despite a certain increase of overpotential, features of the plateaus are not strongly modified, indicating no change in the electrochemical mechanisms with coated magnesium electrodes for both ACC-S and PAQS-CNT composites. In the first case, the important capacity fading is mainly induced by the important polysulphide species

dissolution and to their well-known shuttle to the anode side, as revealed by XPS analysis performed after hours of cycling (Figure S14). For PAQS-CNT composite, the polymer is not completely insoluble and consequently, the cycling capacity progressively decreases. This is however also observed with uncoated magnesium electrodes employed with $\text{Mg}(\text{B}(\text{hfp})_4)_2$ and $\text{Mg}(\text{TFSI})_2\text{-}2\text{MgCl}_2$ electrolytes (Figure S15).

Conclusions and Perspectives

In this work, we propose an innovative protocol to create an alloy layer on the surface of magnesium to unlock the use of non-corrosive chloride-free electrolytes for magnesium batteries. From preliminary galvanostatic polarization measurements to full cells with various positive electrode materials, the as-coated magnesium electrodes exhibit enhanced electrochemical performance. The magnesium surface passivation, which usually precludes any electrochemical activity, does not occur, and reversible magnesium plating and stripping is demonstrated. For this proof-of-concept, liquid gallium was used to create a relatively thick alloy layer. Although gallium is relatively light, the alloy layer impacts the overall energy density (Figures S16-17). Therefore, the coating protocol must be further optimized to create a thinner and more robust gallium-based protective layer. Designing self-healing composite coating could be also achieved with alloy coating based on liquid eutectic compositions.⁵¹ In addition, different types of magnesium electrolytes need to be tested, keeping in mind the final purpose of using carbonate-based electrolytes for benchmarking high-voltage positive electrode materials, together with a detailed understanding of the evolution of both the protective layer and the solid-electrolyte interphase during battery cycling. Overall, this study opens the door for the large-scale application of low-melting-point elements and compounds to protect sensitive metal electrodes such as magnesium and calcium.

Methods

Ga-coated Mg electrodes. Mg-Ga electrodes were prepared in an argon-filled glovebox with <0.5 ppm oxygen and <0.5 ppm H₂O at room temperature. Mg foil (Goodfellow, 99.9%, 250µm) was first polished with a blade to remove the native oxide layer. Then, the coating was made by dropping liquid Ga (from molten ingots, Alfa-Aesar) droplets onto the surface of Mg and spread over until a homogeneous liquid layer was formed. After few hours, the liquid layer reacted with Mg to form a solid alloy layer.

Positive electrode materials. Chevrel phase Mo₆S₈, ACC-S and PAQS-CNT composites were prepared following previous reports.^{40,48–50,52,53} Details on syntheses, characterizations and electrode formulation are provided in the Supplementary Information.

Electrochemical tests. Electrodes were tested in coin-cells (2032, 316L stainless steel) assembled in an argon-filled glove-box, one glass-fibre (Whatman, GF/A) surrounded by two polypropylene membranes (Celgard 2325) was used as a separator and wetted with 100 µL of electrolyte. Tests have been performed mainly in an oven set at 40 °C, and also at room temperature, using research-grade potentiostats (Neware and Bio-Logic).

X-ray diffraction (XRD). Samples were prepared in an Ar-filled glove box and then transfer under a protective airtight polymeric film to limit moisture reaction. XRD measurements in reflection were performed with a Panalytical X'Pert Pro diffractometer operating with Cu K α radiation. For the *operando* XRD measurement in transmission, a specially designed cell using two Be windows acting as both X-ray transparent windows and current collectors was assembled in Ar-filled glovebox. The transmission XRD acquisitions were carried out with a Bruker D8 Discover diffractometer equipped with a rotating anode (Mo-K α radiation) and a

Dectris EIGER2 R 500K detector. In parallel, electrochemical measurements were operated on a BCS potentiostat (Bio-Logic).

Auger electron spectroscopy (AES) and scanning Auger microscopy (SAM). Coated magnesium discs were mechanically cut and then polished by an Ar⁺ ion beam in a cross-section polisher (model IB-09010CP, Jeol Ltd., Tokyo, Japan) operating at 4 keV for 2 hours (working pressure of 1.10^{-4} Pa). Polished discs were transferred without any air exposure into the Auger electron nano probe (JAMP 9500F, Jeol Ltd.) to perform the SAM imaging and the AES analyses of the electrode cross-cut sections. The Auger analyses were carried out under UHV conditions (pressure $< 2.10^{-7}$ Pa), using the following beam energy and current conditions: 10 keV and 8 nA, respectively.

X-ray photoelectron spectroscopy (XPS). Samples were transferred without any air exposure into an Ar-filled glove box ($< 1\text{ppm O}_2$, $< 1\text{ppm H}_2\text{O}$) directly connected to the XPS spectrometer (Thermofischer Scientific Escalab 250 Xi) using focused monochromatized Al-K α radiation ($h\nu = 1486.6$ eV). No sputtering was used to clean the surface to analyze in order to preserve the surface chemistry. The analyzed surface area of the samples was a 650 μm diameter disk. The spectra were fit and analysed in CasaXPS software.

DFT calculation. Periodic calculations were performed within the density functional theory (DFT) framework, using the Vienna ab initio simulation package (VASP) implemented with projector augmented wave pseudopotentials (PAW).^{54,55} Exchange-correlation effects have been accounted for by the generalized gradient approximation (GGA) using the functional of Perdew, Burke and Ernzerhof (PBE).⁵⁶ Surface calculations were performed on Mg₂Ga₅ (100), (010) and (001) slabs. The surrounding environment was described with an implicit solvent using the polarizable continuum model (PCM) as implemented in VASPsol.⁵⁷ To vary the electrode potential, the grand canonical density functional theory (GC-DFT) framework has

been used in association to the homogeneous background method (HBM) as detailed in previous works.⁵⁸ More details can be found in the Supplementary Information section.

References

1. Aurbach, D. *et al.* Prototype systems for rechargeable magnesium batteries. *Nature* **407**, 724–727 (2000).
2. Ponrouch, A. *et al.* Multivalent rechargeable batteries. *Energy Storage Mater.* **20**, 253–262 (2019).
3. Dominko, R. *et al.* Magnesium batteries: Current picture and missing pieces of the puzzle. *J. Power Sources* **478**, (2020).
4. Mohtadi, R., Tutusaus, O., Arthur, T. S., Zhao-Karger, Z. & Fichtner, M. The metamorphosis of rechargeable magnesium batteries. *Joule* **5**, 581–617 (2021).
5. Kopač Lautar, A. *et al.* Electrolyte Reactivity in the Double Layer in Mg Batteries: An Interface Potential-Dependent DFT Study. *J. Am. Chem. Soc.* **142**, 5146–5153 (2020).
6. Kopač Lautar, A., Bitenc, J., Dominko, R. & Filhol, J.-S. Building Ab Initio Interface Pourbaix diagrams to Investigate Electrolyte Stability in the Electrochemical Double Layer: Application to Magnesium Batteries. *ACS Appl. Mater. Interfaces* **13**, 8263–8273 (2021).
7. Rashad, M., Asif, M., Wang, Y., He, Z. & Ahmed, I. Recent advances in electrolytes and cathode materials for magnesium and hybrid-ion batteries. *Energy Storage Mater.* **25**, 342–375 (2020).
8. Jankowski, P. *et al.* Development of Magnesium Borate Electrolytes: Explaining the Success of Mg[B(hfip)4]2 Salt. *Energy Storage Mater.* (2021). doi:10.1016/j.ensm.2021.11.012
9. Son, S. B. *et al.* An artificial interphase enables reversible magnesium chemistry in carbonate electrolytes. *Nat. Chem.* **10**, 532–539 (2018).
10. Sun, Y., Zou, Q., Wang, W. & Lu, Y. C. Non-passivating Anion Adsorption Enables Reversible Magnesium Redox in Simple Non-nucleophilic Electrolytes. *ACS Energy Lett.* **6**, 3607–3613 (2021).
11. Liang, X. *et al.* A facile surface chemistry route to a stabilized lithium metal anode. *Nat. Energy* **2**, 17119 (2017).
12. Choudhury, S. *et al.* Electroless Formation of Hybrid Lithium Anodes for Fast Interfacial Ion Transport. *Angew. Chemie - Int. Ed.* **56**, 13070–13077 (2017).
13. Pang, Q., Liang, X., Kochetkov, I. R., Hartmann, P. & Nazar, L. F. Stabilizing Lithium Plating by a Biphasic Surface Layer Formed In Situ. *Angew. Chemie - Int. Ed.* **57**, 9795–9798 (2018).
14. Tu, Z. *et al.* Fast ion transport at solid-solid interfaces in hybrid in hybrid battery anodes. *Nat. Energy* **3**, 310–316 (2018).
15. Touja, J., Louvain, N., Stievano, L., Monconduit, L. & Berthelot, R. An Overview on Protecting Metal Anodes with Alloy-Type Coating. *Batter. Supercaps* **n/a**, (2021).
16. Davidson, R. *et al.* Formation of Magnesium Dendrites during Electrodeposition. *ACS Energy Lett.* **4**, 375–376 (2019).
17. Davidson, R. *et al.* Mapping mechanisms and growth regimes of magnesium electrodeposition at high current densities. *Mater. Horizons* **7**, 843–854 (2020).
18. Zhao, Y. *et al.* Effect of Mg Cation Diffusion Coefficient on Mg Dendrite Formation. *ACS Appl. Mater. Interfaces* (2022). doi:10.1021/acsami.1c18543

19. Lv, R., Guan, X., Zhang, J., Xia, Y. & Luo, J. Enabling Mg Metal Anodes Rechargeable in Conventional Electrolytes by Fast Ionic Transport Interphase. *Natl. Sci. Rev.* (2019). doi:10.1093/nsr/nwz157
20. Zhao, Y. *et al.* A Bismuth-Based Protective Layer for Magnesium Metal Anode in Noncorrosive Electrolytes. (2021).
21. Zhang, J. *et al.* Rechargeable Mg metal batteries enabled by a protection layer formed in vivo. *Energy Storage Mater.* **26**, 408–413 (2020).
22. He, G., Li, Q., Shen, Y. & Ding, Y. Flexible Amalgam Film Enables Stable Lithium Metal Anodes with High Capacities. *Angew. Chemie - Int. Ed.* **58**, 18466–18470 (2019).
23. Zhang, Q. *et al.* A thermodynamically stable quasi-liquid interface for dendrite-free sodium metal anodes. *J. Mater. Chem. A* 6822–6827 (2020). doi:10.1039/d0ta02016h
24. Yang, Q., Ding, Y. & He, G. An amalgam route to stabilize potassium metal anodes over a wide temperature range. *Chem. Commun.* **56**, 3512–3515 (2020).
25. Moskalyk, R. R. Gallium: The backbone of the electronics industry. *Miner. Eng.* **16**, 921–929 (2003).
26. Mir, S., Vaishampayan, A. & Dhawan, N. A Review on Recycling of End-of-Life Light-Emitting Diodes for Metal Recovery. *Jom* (2022). doi:10.1007/s11837-021-05043-9
27. Zhao, Z., Yang, Y., Xiao, Y. & Fan, Y. Recovery of gallium from Bayer liquor: A review. *Hydrometallurgy* **125–126**, 115–124 (2012).
28. Niu, J., Zhang, Z. & Aurbach, D. Alloy Anode Materials for Rechargeable Mg Ion Batteries. **2000697**, 1–33 (2020).
29. Wang, L. *et al.* High-Rate and Long Cycle-Life Alloy-Type Magnesium-Ion Battery Anode Enabled Through (De)magnesiumation-Induced Near-Room-Temperature Solid–Liquid Phase Transformation. *Adv. Energy Mater.* **9**, 1902086 (2019).
30. Yu, Y. *et al.* Instability at the Electrode/Electrolyte Interface Induced by Hard Cation Chelation and Nucleophilic Attack. *Chem. Mater.* **29**, 8504–8512 (2017).
31. Tutusaus, O., Mohtadi, R., Singh, N., Arthur, T. S. & Mizuno, F. Study of Electrochemical Phenomena Observed at the Mg Metal/Electrolyte Interface. *ACS Energy Lett.* **2**, 224–229 (2017).
32. Connell, J. G. *et al.* Tuning the Reversibility of Mg Anodes via Controlled Surface Passivation by H₂O/Cl⁻ in Organic Electrolytes. *Chem. Mater.* **28**, 8268–8277 (2016).
33. Yan, Q. *et al.* A Perspective on interfacial engineering of lithium metal anodes and beyond. *Appl. Phys. Lett.* **117**, 080504 (2020).
34. Whang, G. *et al.* Avoiding dendrite formation by confining lithium deposition underneath Li–Sn coatings. *J. Mater. Res.* **36**, 797–811 (2021).
35. Levi, M. D. *et al.* Kinetic and Thermodynamic Studies of Mg²⁺ and Li⁺ Ion Insertion into the Mo₆S₈ Chevrel Phase. *J. Electrochem. Soc.* **151**, A1044–A1051 (2004).
36. Levi, E. *et al.* Phase Diagram of Mg Insertion into Chevrel Phases, Mg_xMo₆T₈ (T = S, Se). 1. Crystal Structure of the Sulfides. *Chem. Mater.* **18**, 5492–5503 (2006).
37. Zhao-Karger, Z. & Fichtner, M. Magnesium-Sulfur battery: its beginning and recent progress. *MRS Commun.* 1–15 (2017).
38. Kong, L. *et al.* A Review of Advanced Energy Materials for Magnesium–Sulfur Batteries. *ENERGY Environ. Mater.* **1**, 100–112 (2018).
39. Mao, M., Gao, T., Hou, S. & Wang, C. A critical review of cathodes for rechargeable Mg batteries. *Chem. Soc. Rev.* **47**, 8804–8841 (2018).
40. Bitenc, J. *et al.* Anthraquinone-Based Polymer as Cathode in Rechargeable Magnesium Batteries. *ChemSusChem* **8**, 4128–4132 (2015).
41. Bitenc, J. *et al.* Poly(hydroquinoyl-benzoquinonyl sulfide) as an active material in Mg and Li organic

- batteries. *Electrochem. commun.* **69**, 1–5 (2016).
42. Fan, X. *et al.* A Universal Organic Cathode for Ultrafast Lithium and Multivalent Metal Batteries. *Angew. Chemie Int. Ed.* **57**, 7146–7150 (2018).
 43. Bitenc, J. *et al.* Electrochemical Performance and Mechanism of Calcium Metal-Organic Battery. *Batter. Supercaps* **4**, 214–220 (2021).
 44. Dong, H. *et al.* High-power Mg batteries enabled by heterogeneous enolization redox chemistry and weakly coordinating electrolytes. *Nat. Energy* **5**, 1043–1050 (2020).
 45. Pan, B. *et al.* Polyanthraquinone-Based Organic Cathode for High-Performance Rechargeable Magnesium-Ion Batteries. *Adv. Energy Mater.* **6**, 2–4 (2016).
 46. Pavčnik, T., Bitenc, J., Pirnat, K. & Dominko, R. Electrochemical Performance of Mg Metal-Quinone Battery in Chloride-Free Electrolyte. *Batter. Supercaps* **4**, 815–822 (2021).
 47. Han, Y. *et al.* High-performance Mg–organic batteries based on hybrid MgCl₂–LiCl/THF electrolytes. *Energy Storage Mater.* **46**, 300–312 (2022).
 48. Gao, T. *et al.* Reversible S₀/MgS_x Redox Chemistry in a MgTFSI₂/MgCl₂/DME Electrolyte for Rechargeable Mg/S Batteries. *Angew. Chemie* **129**, 13711–13715 (2017).
 49. Gao, T. *et al.* Thermodynamics and Kinetics of Sulfur Cathode during Discharge in MgTFSI₂–DME Electrolyte. *Adv. Mater.* **30**, (2018).
 50. Meng, Z. *et al.* Alloys to Replace Mg Anodes in Efficient and Practical Mg-Ion/Sulfur Batteries. *ACS Energy Lett.* **4**, 2040–2044 (2019).
 51. Song, M. *et al.* A self-healing room-temperature liquid eutectic GaSn anode with improved wettability for advanced Mg ion batteries. *Chem. Eng. J.* **435**, 134903 (2022).
 52. Choi, S.-H. *et al.* Role of Cu in Mo₆S₈ and Cu Mixture Cathodes for Magnesium Ion Batteries. *ACS Appl. Mater. Interfaces* **7**, 7016–7024 (2015).
 53. Song, Z., Zhan, H. & Zhou, Y. Anthraquinone based polymer as high performance cathode material for rechargeable lithium batteries. *Chem. Commun.* 448–450 (2009). doi:10.1039/B814515F
 54. Kresse, G. & Hafner, J. Ab initio molecular dynamics for liquid metals. *Phys. Rev. B* **47**, 558–561 (1993).
 55. Blöchl, P. E. Projector augmented-wave method. *Phys. Rev. B* **50**, 17953–17979 (1994).
 56. Perdew, J. P., Burke, K. & Ernzerhof, M. Generalized Gradient Approximation Made Simple. *Phys. Rev. Lett.* **77**, 3865–3868 (1996).
 57. Mathew, K., Sundararaman, R., Letchworth-Weaver, K., Arias, T. A. & Hennig, R. G. Implicit solvation model for density-functional study of nanocrystal surfaces and reaction pathways. *J. Chem. Phys.* **140**, 84106 (2014).
 58. Kopač Lautar, A., Hagopian, A. & Filhol, J.-S. Modeling interfacial electrochemistry: concepts and tools. *Phys. Chem. Chem. Phys.* **22**, 10569–10580 (2020).
 59. Lv, R., Guan, X., Zhang, J., Xia, Y. & Luo, J. Enabling Mg metal anodes rechargeable in conventional electrolytes by fast ionic transport interphase. *Natl. Sci. Rev.* **7**, 333–341 (2020).
 60. Li, Y. *et al.* Formation of an Artificial Mg²⁺-Permeable Interphase on Mg Anodes Compatible with Ether and Carbonate Electrolytes. (2021). doi:10.1021/acsami.0c22520
 61. Zhang, R. *et al.* An artificial interphase enables the use of Mg(TFSI)₂-based electrolytes in magnesium metal batteries. *Chem. Eng. J.* **426**, 130751 (2021).
 62. Monkhorst, H. J. & Pack, J. D. Special points for Brillouin-zone integrations. *Phys. Rev. B* **13**, 5188–5192 (1976).
 63. Hagopian, A., Falcone, A., Ben Yahia, M. & Filhol, J.-S. Ab initio modelling of interfacial electrochemical properties: beyond implicit solvation limitations. *J. Phys. Condens. Matter* **33**, 304001

(2021).

Acknowledgements

The authors gratefully acknowledge financial support from the French National Research Agency (project MISTRAL, ANR-19-CE05-0013, and Labex STORE-EX, ANR-10-LABX-76-01), Cellule Energie CNRS (project PEPS DIBAPA). O. L., J. B. and R. D. would like to thank the European Union's Horizon 2020 research and innovation program under the Marie Skłodowska-Curie grant agreement No. 860403. J.B and R. D. would also like to acknowledge support of Slovenia Research Agency under research programs P2-0393 and P2-0423.

Author contributions

C. P. carried out the electrode coating and the electrochemical characterizations, the *operando* XRD measurement (with J.-N. C) and the surface and cross-section analysis (with D. F., J.-B. L., J. A. and R. D); A. H. and J.-S. F. performed and discussed the DFT calculations; O. L, J. B and R. D. provided the PAQS-CNT composite and characterized its electrochemical behaviour; R. B. supervised the overall study; C. P. L. S. and R. B. wrote the manuscript and all authors discussed the experiments and final manuscript.

Additional information

Supplementary information is available in the online version of the article. Correspondence and requests for materials could be addressed to R. B.

Competing financial interests

The authors declare no competing financial interests.